Semiclassical dynamics of the van der Waals states in $O_3(X^1A_1)$

Marc Joyeux
Laboratoire de Spectrométrie Physique (CNRS UMR 5588), Université Joseph Fourier-Grenoble I, BP 87, 38402 St. Martin d'Hères Cedex, France

Reinhard Schinke and Sergy Yu. Grebenshchikov[a)]
Max-Planck-Institut für Strömungsforschung, D-37073 Göttingen, Germany

(Received 5 December 2003; accepted 28 January 2004)

We present the analysis and the semiclassical quantization of the van der Waals states of ozone in the ground electronic state $X\,^1A_1$. Progressions of these states dominate the spectrum of O_3 at threshold. Periodic orbits are used to perform assignment and quantization of the vibrational states. Semiclassical quantization is numerically accurate despite the fact that the classical phase space is chaotic while the nodal patterns of the quantum mechanical wave functions are regular. The lifetimes of recombination of the van der Waals states into the ''normal'' ozone are also discussed.
 [DOI: 10.1063/1.1687671]

I. INTRODUCTION

Molecular eigenstates near dissociation threshold are the subject of intensive investigations in the field of chemical dynamics (see Refs. 1–3, and references therein). Nonlinear anharmonic coupling between the internal degrees of freedom, whose influence grows with increasing deviations from the equilibrium and thus with energy, substantially changes the properties of highly energized polyatomic molecules. As a result of progress in computational quantum chemistry,[4] accurate potential energy surfaces (PESs) can now be constructed for small polyatomics even far away from equilibrium and reliable predictions of unusual properties of the weakly bound threshold states can be made.[1] New dynamical features near dissociation can be grouped into two broad categories. First, assignment of the eigenstates becomes intricate. For example, the normal mode assignment, appropriate near the ground vibrational state, often loses its meaning at high excitation energies.[5] At best, new quantum numbers can be introduced which still uniquely characterize eigenstates [the well studied normal- to local mode transition in triatomics (Refs. 6 and 7, and references therein) serves as an example]. More generic is a gradual transition from an assignable spectrum to an ensemble of irregular eigenstates characterized only by an exact symmetry of the system, the energy, and the total angular momentum. This transition is thoroughly documented by Jost *et al.* in the experimental spectroscopic studies of the bound states of nitrogen dioxide.[8–10] The other distinctive characteristic of the threshold region is that new groups of vibrational eigenstates appear in the spectrum. Typically, they are the result of ''bifurcations'' in the existing progressions triggered by sudden changes in the classical phase space.[3] Such ''bifurcations'' were studied for many triatomic molecules including HCP,[2] HOCl,[11] H_3^+,[12] and HOBr.[13] Alternatively, new progressions of molecular states can form in those regions of the intramolecular potential, which become accessible only at threshold. A striking example is furnished by ozone in the ground electronic state. Recently, we investigated the bound states of this molecule on a new high-quality *ab initio* global PES.[14] The main feature of the PES in the dissociation $O\cdots O_2$ channel is a van der Waals (vdW) minimum situated approximately 200 cm^{-1} below the asymptote. Using accurate quantum mechanical calculations, it was shown[14] that the shallow vdW well supports progressions of vibrational states. For all vdW states, the average distance between the O atom and the O_2 fragment exceeds 5 bohr. These states exist in the same energy range as the vibrational states of ''normal'' ozone. However, they retain a large degree of independence of the latter: Mixings between the two types of eigenstates are rather weak. Appearing only 150 cm^{-1} below the quantum mechanical threshold (D_0), vdW states become the dominant species at D_0 and increase the spectral density in a nonrotating molecule to 0.8 per cm^{-1}. The role of vdW states in reactions above dissociation threshold, in particular the ozone formation and the oxygen exchange, are currently under extensive scrutiny.

In the present article the vdW states in ozone are analyzed from a semiclassical viewpoint. Isotopomer $^{16}O\cdots{}^{18}O_2$ is chosen as an example. Quantum mechanical calculations showed that the vibrational assignment is straightforward for most of the eigenstates. However, new types of eigenstates are observed near dissociation threshold and we apply the semiclassical approximation in order to clarify the nature of the strange vibrational states and to trace the origin of the quantum ''bifurcations.'' To this end, a detailed study of the classical phase space and the quantum/classical correspondence is undertaken. Semiclassical calculations are significantly alleviated by the fact that the molecular motion in the vdW well is two dimensional. It is confined to the two internal degrees of freedom, the $O\cdots O_2$ stretch, R, and the bending (or hindered rotation) coordinate, γ.[14] As will be shown below, the O_2 fragment in the ground vibrational state is not

a)Author to whom correspondence should be addressed. Electronic mail: sgreben@gwdg.de

involved in the dynamics and can be effectively decoupled from R and γ.

We investigate the correspondence between the morphology of the wave functions and the periodic orbits (POs), i.e. closed classical trajectories on which the molecule remains trapped. It is well known,[3,15,16] that in the systems, which are ''not too chaotic,'' the building blocks of the phase space are the fundamental families of the POs. One usually distinguishes between the stable and unstable POs. Loosely speaking, each stable PO lies at the center of a certain region in the phase space while unstable POs separate different regions. Recent studies of HCP (Ref. 2) and DCP,[17] HOCl (Ref. 18) and HOBr (Ref. 13) confirm that the quantum mechanical spectrum of these molecules, in the entire energy range extending from the bottom of the potential well up to very high energies reflects the deformations of the stable POs. In this paper we present an example of a system with clearly assignable eigenstates but apparently chaotic classical mechanics and unstable periodic orbits. It is shown that a quantization, usually applicable for integrable systems, can be performed along unstable POs and gives reasonable estimation of quantum eigenenergies.

Semiclassical analysis of the vdW dynamics also provides information on the accuracy of trajectory calculations at the dissociation threshold of ozone. An effort was made recently to understand the anomalous ''mass-independent'' isotope effect in ozone formation and exchange reactions[19–21] using classical mechanics.[22–24] While indispensable in treatment of the reaction complex in high total angular momentum states, the classical approach ignores the existence of the quantum mechanical threshold D_0. This well-known drawback obscures the results of trajectory calculations, especially if—as in ozone—low excess energies up to 200 cm^{-1} above D_0 are of interest.[24] Direct comparison of the phase space structures with the vdW wave functions enables one to point out those features which classical mechanics describes properly and to indicate discrepancies. To this end, the lifetimes of the vdW states with respect to recombination into the main ozone wells are studied. It is shown that the chaotic classical mechanics, being adequate for the description of the average recombination times, cannot reproduce the fluctuations of the lifetimes of the regular quantum mechanical eigenstates.

The rest of the paper is organized as follows: In Sec. II the adiabatic two-dimensional (2D) model Hamiltonian for vdW states in $^{16}O\cdots{}^{18}O_2$ is presented. The eigenstates of this operator are described and the quality of the 2D approximation is assessed. Efficient semiclassical quantization of the 2D model using selected periodic orbits is described in Sec. III and in the Appendix. The phase space is further analyzed in Sec. IV by means of the Poincaré surface of section, while the recombination lifetimes of the vdW states and the quantum/classical correspondence are discussed in Sec. V. Section VI concludes.

II. ADIABATIC MODEL

A nonrotating ozone molecule in the vdW region in one dissociation channel $^{16}O\cdots{}^{18}O_2$ is described in Jacobi coordinates: R is the distance between the $^{18}O_2$ moiety and the third oxygen atom, r is the $^{18}O_2$ stretching coordinate, and γ is the angle between $\mathbf{R}$ and $\mathbf{r}$. The shallow double-well vdW minimum in the asymptotic channel is located at $R_0=5.3a_0$, $r_0=2.28a_0$, and $\gamma_0=53.7°$ and 126.3°. The vdW region is separated from the main ozone well by a low ($\sim$80 cm^{-1}) barrier at $R_b=4.5a_0$. This barrier marks the symbolic border between the asymptotic region and the main ozone well. The vibrational spectrum in the vdW region was previously calculated in three dimensions (3D) and discussed in Ref. 14. The fundamental frequencies associated with the dissociation coordinate R and the bending γ are $\omega_R \approx 40\,cm^{-1}$ and $\omega_\gamma \approx 60\,cm^{-1}$, respectively. They are more than one order of magnitude smaller than the vibrational frequency of the nearly free $^{18}O_2$ diatom, $\omega_r \approx 1465\,cm^{-1}$. Near the first dissociation threshold, the wave functions of vdW states are entirely two-dimensional, with excitations solely in R and γ (see Fig. 2 in Ref. 14). Thus, it is legitimate to apply an adiabatic approximation to the vdW region, separate the high frequency r vibration from the other two, and consider the vdW dynamics for the resulting 2D Hamiltonian. Of course, the adiabatic approximation is valid only in the asymptotic region, for $R \geqslant R_b$.

Adiabatic separation proceeds along a familiar line.[25] The full 3D Hamiltonian in Jacobi coordinates,

$$H_{3D} = -\frac{1}{2\mu_R}\frac{\partial^2}{\partial R^2} - \frac{1}{2\mu_r}\frac{\partial^2}{\partial r^2} + B(R,r)j^2 + V(R,r,\gamma) \tag{1}$$

is averaged over the vibrational state of the $^{18}O_2$ oscillator. Here $\mu_{R,r}$ are the reduced masses for R and r, respectively; $B(R,r)$ is the coordinate dependent rotational constant; j is the angular momentum operator for the diatom; $V(R,r,\gamma)$ is the *ab initio* PES of ozone in the ground electronic state, and we set $\hbar \equiv 1$. For $R \geqslant R_b$, the total 3D wave function can be written as

$$\Psi_{3D} = \psi_n(r|R,\gamma)\Phi(R,\gamma), \tag{2}$$

where $\psi_n(r|R,\gamma)$ is the nth eigenfunction of the $^{18}O_2$ diatom which solves the one-dimensional Schrödinger equation

$$\left[-\frac{1}{2\mu_r}\frac{\partial^2}{\partial r^2} + V(r|R,\gamma)\right]\psi_n(r|R,\gamma) = \epsilon_n(R,\gamma)\psi_n(r|R,\gamma) \tag{3}$$

for fixed R and γ. The eigenenergy $\epsilon_n(R,\gamma)$ plays the role of a potential for the 2D motion in the (R,γ) plane. In this paper, we are interested in the ground vibrational state of $^{18}O_2$, $n=0$, so that the effective 2D Hamilton operator for R and γ acting onto $\Phi(R,\gamma)$ can be written as

$$H_{2D} = -\frac{1}{2\mu_R}\frac{\partial^2}{\partial R^2} + B(R,\langle r\rangle)j^2 + \epsilon_0(R,\gamma), \tag{4}$$

where $\langle r\rangle$ is an average bond length of $^{18}O_2$ in the ground state and $R \geqslant R_b$. Eigenvalues of this operator approximate the vdW states with $n=0$ of the full 3D Hamiltonian, Eq. (1).

In practice, we first solve the one-dimensional Schrödinger equation (3) on a dense grid of fixed values of R

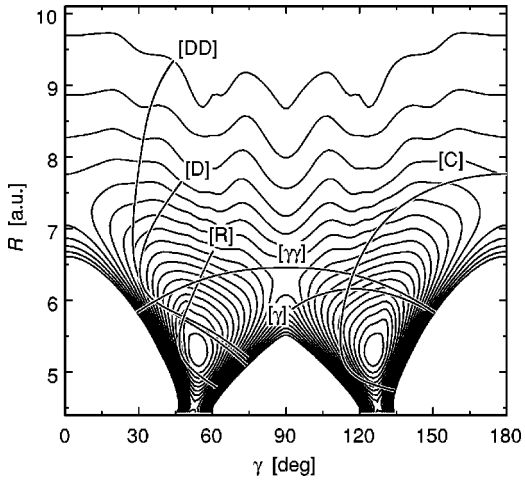

FIG. 1. Adiabatic two-dimensional potential $\epsilon_0(R,\gamma)$ for the ozone molecule $^{16}O\cdots{}^{18}O_2$. The lowest shown contour lies at $E=10\,\mathrm{cm}^{-1}$, and the spacing between contours is $\Delta E=10\,\mathrm{cm}^{-1}$. Also presented are the examples of periodic orbits belonging to the six families described in the text.

$\in[4.4,15.0]a_0$ and $\gamma\in[0,\pi]$ to obtain the 2D ''potential'' $\epsilon_0(R,\gamma)$. The energies on the grid are subsequently interpolated using cubic splines. The resulting adiabatic potential is depicted in Fig. 1. It has two minima along γ separated by a barrier ridge with the saddle point at $\gamma=90°$ and $R=6.3a_0$. Just like the original ''bare'' potential, the minima of ϵ_0 are symmetric: The diatom $^{18}O_2$ is homonuclear. There are two minima and five saddle points on the surface. The lowest, with respect to the minima, are the saddle points at $R=R_b$ and $\gamma=52°$; 128°; their height is 80 cm^{-1}. The minimum energy path (MEP) through each of them leads into the main ozone well. The saddle separating the two vdW minima lies 125 cm^{-1} above the minima. The highest are the saddle points at linearity ($\gamma=0°$; 180° and $R=7.4a_0$); their energy is 155 cm^{-1}. On this scale, dissociation threshold is found at $D_0=205\,\mathrm{cm}^{-1}$. Only energies below D_0 are considered.

One clearly sees that as the potential energy approaches dissociation threshold, the 2D PES loses smoothness: Wavy structures, first visible at $E\approx120\,\mathrm{cm}^{-1}$, become pronounced at D_0. In fact, these structures are also present in the original *ab initio* potential, and are transferred intact into the adiabatic PES. As was shown previously,[26] as many as 9 electronic states of ozone asymptotically converge to the lowest dissociation threshold. This limits the accuracy of the *ab initio* calculations which include only the ground electronic state.[27] The nonmonotonic behavior of the potential energy in the asymptotic channel and the corresponding wavy structures in Fig. 1 serve as a reminder of the limited accuracy of the ozone interaction potential at dissociation threshold.

The 2D adiabatic potential $\epsilon_0(R,\gamma)$ is used in the classical and quantum mechanical calculations presented in this paper. In quantum mechanics, the 2D Hamilton operator, Eq. (4), is diagonalized numerically using filter diagonalization.[28,29] The potential optimized[30] sinclike[31] DVR grid in R, consisting of 200 points, ranges from $4.4a_0$ to $16.0a_0$. In γ, a Gauss–Legendre DVR grid with 200 points was used. About 70 000 Chebyshev iterations were necessary to obtain a fully converged spectrum of bound states.

The quality of the adiabatic model can be assessed by comparing the 2D vdW spectrum with that of the ''restricted'' 3D calculations of Ref. 14. We remind the reader that the restricted calculations were performed[14] in a single dissociation channel of ozone in Jacobi coordinates; the full Hamiltonian was set on a 3D grid which, in R and γ, had the same extensions as described in the preceding paragraph. Thus, the numerical solution to the ''restricted'' problem serves as a benchmark for the 2D adiabatic approximation.

State-to-state comparison demonstrates that the adiabatic model is excellent in the vdW region of the potential. The number of eigenstates in the 2D calculations (22) coincides with that in the restricted 3D calculations. The two fundamental frequencies are also accurately reproduced. Assignment of the wave functions and the energetic order of states are the same in 2D and in 3D. Adiabatic separation of the O_2 vibration introduces an error smaller than 0.5 cm^{-1}. This uncertainty is much less than either ω_R or ω_γ.

Examples of 2D wave functions in the three main vdW progressions are presented in Fig. 2. Their 3D counterparts

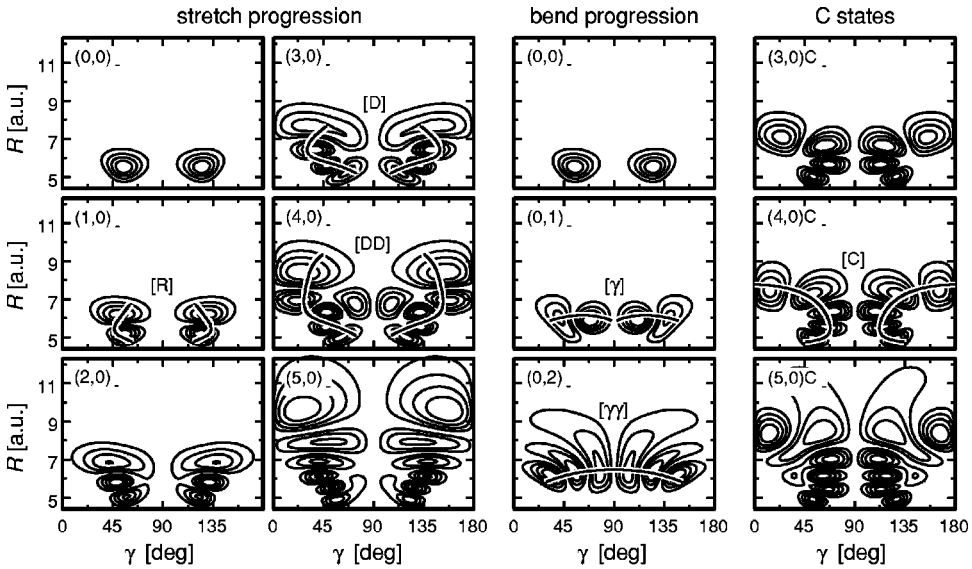

FIG. 2. Examples of the wave functions of vdW states in three progressions. Additionally, the periodic orbits are shown, which are used in the semiclassical quantization.

can be found in Fig. 2 of Ref. 14. The vdW states possess a clear nodal structure so that the two main progressions, the stretch and the bend, can be easily identified. Incidentally, we note that 16 out of 22 states are pure overtones, and only six states are combinations of the bending and stretching excitations. The eigenstates are delocalized between the two vdW wells along the angular coordinate. Those which have a nodal line at the saddle $\gamma=90°$ are antisymmetric with respect to the transformation $\gamma\rightarrow 180°-\gamma$ and are denoted with an additional index "$-$." The symmetric states have the index "$+$." Figure 2 shows that close to dissociation threshold, another progression appears in addition to the stretching and bending ones. The same states are found in three dimensions, both in the restricted and global calculations of ozone.[14] The nature of these states will be analyzed using the semiclassical analysis presented below.

III. PERIODIC ORBIT QUANTIZATION

We build the semiclassical approximation to the quantum mechanical spectrum using the POs with the shortest periods. The POs were located using two-point boundary value solvers, as described in Sec. II of Ref. 32. Recombination of the vdW species into the main ozone, energetically allowed for $E\geqslant 80\,\mathrm{cm}^{-1}$, adds complexity to the search of the POs: Already the initial guess for a given PO should be sufficiently precise. This is achieved by using an accurate continuation in energy.

At very low energies (a few cm^{-1} above the bottom of the well), there exist two fundamental families of stable POs, one corresponding to the pure bending ($[\gamma]$) and the other to the pure stretching oscillations ($[R]$). Evolution of these POs with energy is illustrated using the continuation/bifurcation diagram[16] in Fig. 3. The diagram shows how the classical frequencies change from the bottom of the vdW well to the dissociation threshold. The orbits in the fundamental $[R]$ family [Fig. 3(a)] can be followed up to relatively high energies although they are for the most part unstable. Above $E=154\,\mathrm{cm}^{-1}$ they cease to exist and are replaced by another family of POs called $[D]$, which appears at $E=139\,\mathrm{cm}^{-1}$ [Fig. 3(a)]. Such crossovers were previously analyzed in the vibrational spectra of HCP (Ref. 2) and HOCl (Ref. 11) in terms of saddle-node bifurcations. The $[D]$ family is possibly also born in a saddle-node bifurcation, but the structure of the phase space, discussed in the next section, rendered the detailed bifurcation analysis impossible. Geometrically, the $[D]$ orbits resemble greatly those belonging to the $[R]$ family (cf. Fig. 1). They disappear at 177 cm^{-1} and a third family of stretching POs, $[DD]$, takes their place at 172 cm^{-1}. This family exists only in a short energy interval near dissociation threshold. The stretching mode plays the role of the dissociation coordinate for the vdW molecule and therefore it is strongly anharmonic: As the energy increases from $E=0$ to $E=200\,\mathrm{cm}^{-1}$, the frequency of $[R]$ (and, then, $[D]$ and $[DD]$) drops by about a factor of 7.

Evolution of the bending POs is illustrated in Fig. 3(b). The fundamental family $[\gamma]$ is stable and easy to locate up to $E=177\,\mathrm{cm}^{-1}$. It is the only short-period bending PO below the isomerization barrier at $\gamma=90°$ (see Fig. 1). Above this barrier ($E>125\,\mathrm{cm}^{-1}$), the bending motion is delocalized between the two symmetric vdW wells. The corresponding family of orbits, called $[\gamma\gamma]$, is born at $E=145\,\mathrm{cm}^{-1}$. This family replaces the $[\gamma]$ POs and survives up to dissociation threshold. The anharmonicity of the $[\gamma]$ family matches that of the dissociation mode $[R]$. This is the consequence of the double-well shape of the angular potential: The anharmonicity increases as the energy approaches the top of the isomerization barrier. In contrast, the frequency of the $[\gamma\gamma]$ family above this barrier is nearly constant.

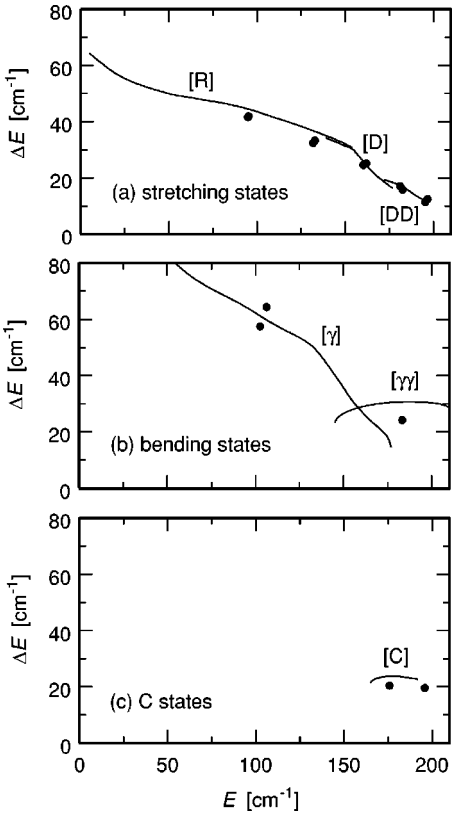

FIG. 3. Frequencies of the periodic orbits (solid lines) as functions of energy: (a) stretching families; (b) bending families; (c) circular family. Dots correspond to the energy differences between neighboring quantum mechanical states in the three pure progressions.

In addition to the bending and stretching POs, one observes at high energies a different family of orbits with short periods [Fig. 3(c)]. These orbits are born at the saddle points at linearity. In the (R,γ) plane, they have a shape similar to that of a quarter of a circle (Fig. 1). For this reason we call them $[C]$ (for "circular"). The energy of the saddles at linearity is 155 cm^{-1}, and the $[C]$ family is observed in the range $E\in[165,192]\,\mathrm{cm}^{-1}$.

The six families of orbits described above are the relevant objects for a semiclassical analysis. There are several indications that these POs make the major contribution to the quantum mechanical eigenstates. A corroborating evidence comes, for example, from the comparison of the classical bifurcation diagram with its quantum mechanical counterpart (Fig. 3). The quantum diagram is constructed from the energy differences between the successive states belonging to the same progression. The states are either symmetric or antisymmetric with respect to $\gamma=90°$, and the energy differences in Fig. 3 are taken between the states from the same

TABLE I. Semiclassical quantization of the vdW spectrum of $^{16}O\cdots^{18}O_2$.

Assignment	E_{sc}, cm^{-1a}	E_{sc}, cm^{-1b}	E_{qm}, cm^{-1c}	Δ_{qm}, cm^{-1d}	Stability of POs[e]
$(0,0)_{+/-}$	75	73	72.8	0.2	s/s
$(1,0)_{+/-}$	114	115	114.5	0.5	u/s
$(0,1)_{+/-}$	138	134	133.9	7.1	u/s
$(2,0)_{+/-}$	150	150	147.5	1.5	u/u
$(1,1)_{+/-}$	⋯	161	162.0	5.1	u/u
$(0,2)_{+}$	170	166	170.1		u/u
$(3,0)_{+/-}$	172	174	172.4	2.0	s/u
$(2,1)_{+}$	⋯	181	182.1		u/u
$(4,0)_{C}$	176	182	184.9		u/u
$(4,0)_{+/-}$	194	193	188.8	0.9	u/u
$(1,2)_{+}$	⋯	184	191.9		u/u
$(0,2)_{-}$	193	193	194.4		u/u
$(3,1)_{+/-}$	⋯	203	202.6	9.3	u/s
$(5,0)_{+/-}$	209	209	200.7	1.9	u/s

[a]Semiclassical energy from Eq. (A5).
[b]Semiclassical energy from Eq. (A9).
[c]For the states split by tunneling, the center of the tunneling doublet is given.
[d]Tunneling splitting between the states with the same assignment but different parities.
[e]Quantizing POs (stretching/bending families) are marked as stable (*s*) or unstable (*u*).

symmetry block. The only exception is the energy difference between the two bending states $(0,2)_+$ and $(0,2,)_-$ [the rightmost point in Fig. 3(b)] which lie above the barrier between the two vdW wells and are localized around the PO $[\gamma\gamma]$. Each difference is plotted at the arithmetic average energy of the two states. The bending, stretching, and circular progressions are shown in Fig. 3. The agreement between the quantum mechanical energy differences and the frequencies of the corresponding POs is very good, especially for the stretching progression [Fig. 3(a)], which is only slightly perturbed by tunneling between the symmetric vdW wells.

Furthermore, the quantum mechanical eigenfunctions are localized near these short-period POs, as illustrated in Fig. 2. For the pure states in the bending and stretching progressions, the respective orbits pass exactly through the nodes of the probability density in the vdW wells. For the circular progression, which does not have analogs at low energies, the correspondence is equally good.

The arguments presented above suggest that one can use these POs for semiclassical quantization. The quantization scheme, which is an alternative to the well-known Einstein–Brillouin–Keller prescription for integrable systems and relies exclusively on POs belonging to the fundamental families, is described in the Appendix. Loosely speaking, the quantization rule, Eq. (A9), for a state (n_R,n_γ) amounts to putting n_R quanta of excitation in a stretching PO, and n_γ quanta of excitation in a bending PO followed by the averaging over the different ways in which the energy partitioning can be achieved. The results of the semiclassical quantization are compared with the quantum mechanical vdW eigenenergies in Table I. The semiclassical approximation is rather accurate, especially for the pure progressions. This validates the assumed correspondence between the PO families and the quantum progressions. As the energy increases, the stretching states are sequentially quantized by the $[R]$, $[D]$, and $[DD]$ families. Similarly, the quantization of bending states switches from the $[\gamma]$ to the $[\gamma\gamma]$ family. The circular state $(4,0)_C$ is accurately quantized with the $[C]$ orbit. For most states, the accuracy of the semiclassical results is limited by tunneling effects, which are not taken into account in the quantization condition.

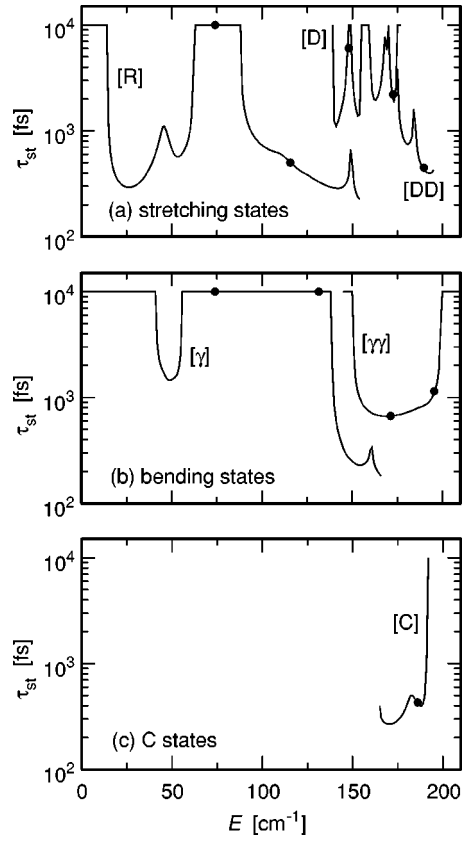

FIG. 4. Energy dependencies of the stability times of the periodic orbits in (a) stretching families; (b) bending families; (c) $[C]$ family. The (infinite) τ_{st} for stable POs is set to 10^4 fs. Black dots mark the energies of the quantum mechanical states quantized with the respective orbits. Positions of the dots along the vertical axis are arbitrary.

IV. CLASSICAL PHASE SPACE OF THE VDW WELLS

Above considerations suggest that the phase space in the vdW region should be regular. Indeed, the eigenenergies are reasonably well reproduced with a simple PO quantization, and each eigenfunction is localized around a single orbit. The analysis of the stability of the quantizing POs indicates, however, that the classical vdW dynamics in ozone is more complicated. Stability in two dimensions is characterized by the stability parameters $\lambda_{1,2}$, which are the eigenvalues of the monodromy matrix.[33] If the $\lambda_{1,2}$ are complex and lie on a unit circle in the complex plane, the PO is said to be stable. If the stability parameters are real, the orbit is unstable. In what follows, we consider the stability *time* of the PO defined through its largest real eigenvalue and period $T(E)$,

$$\tau_{st}(E)=\frac{T(E)}{\ln(\max[\lambda_{1,2}])}. \tag{5}$$

If the orbit is stable, τ_{st} is infinite. The stability times for the POs discussed in the previous section are depicted in Fig. 4.

For stable POs, $\tau_{st}=10^4$ fs is set for plotting purposes. Orbits in each family change their stability as energy increases. The most dramatic variations in τ_{st} are observed in the stretching families [Fig. 4(a)]. The fundamental family $[R]$ loses stability 15 cm^{-1} above the bottom of the vdW well, with τ_{st} quickly dropping down to 300 fs (for comparison, the period at this energy is about 600 fs). The $[R]$ family becomes stable in a short energy window and then its stability degrades again until the orbit can no longer be located. Two high-energy stretching families, $[D]$ and $[DD]$ are for the most part unstable, although τ_{st} strongly oscillates with E. Possibly, these oscillations indicate a cascade of bifurcations which these orbits undergo. The bending motion in the vdW wells [Fig. 4(b)] is much more stable than the stretch, at least up to two thirds of the dissociation energy. The family $[\gamma]$ is stable (with one minor fluctuation) almost until it disappears, while the $[\gamma\gamma]$ family remains slightly unstable up to dissociation threshold. Finally, the family $[C]$ [Fig. 4(c)], existing only near threshold, is unstable. It gains stability only at the highest energy at which it can be located.

The global phase space dynamics of the vdW ozone is analyzed next using the Poincaré surfaces of section (PSOSs) (R,p_R) and (γ,j) (here p_R and j are the momenta conjugate to R and γ, respectively). The PSOS (R,p_R) for a given energy E is computed at a plane in the phase space defined by $\gamma^*=54.2°$. As the classical particle moves in the vdW region, one collects the coordinates R and momenta p_R of the successive intersections with the plane. Only those intersections are considered, for which $j>0$. The PSOS (γ,j) is defined in a similar way, by setting the plane at $R^*=5.29a_0$ and selecting the intersections with $p_R>0$. Both R^* and γ^* are chosen close to the equilibrium in one of the vdW wells.

PSOS enables one to locate the phase space regions with regular and chaotic dynamics. The easiest way to obtain the image of the phase space is to launch many randomly selected trajectories at a given energy, and to analyze the traces they leave in the PSOSs. For a regular trajectory, the intersections with the fixed plane lie on a smooth curve. This smooth curve becomes an irregular scatter of points if the trajectory is chaotic. Surfaces of section, presented in Fig. 5, are recorded at $E=70\,cm^{-1}$, i.e., 10 cm^{-1} below the top of the barrier separating the vdW region from the main ozone wells. The PSOS (γ,j) [Fig. 5(a)] consists of two separate regions corresponding to two symmetric and—at this energy—disconnected vdW wells in the asymptotic channel. Each PSOS in Fig. 5 is composed of three trajectories, demonstrating different types of motion. Two trajectories in the PSOS (γ,j) in Fig. 5(a) are irregular, and their intersections with the fixed plane sample the phase space in either of two vdW wells without any apparent systematics. The third trajectory, confined to a narrow strip close to the energy envelope of the PSOS in the left vdW well, is not chaotic: The points are regularly organized. This trajectory belongs to an island of regularity around the stable PO of the $[\gamma]$ family. The size of this island is illustrated with the PSOS (R,p_R) in Fig. 5(b). Again, only three trajectories are shown. While the irregular one erratically wanders through the phase space, the other two outline the approximate border of the regular phase space.

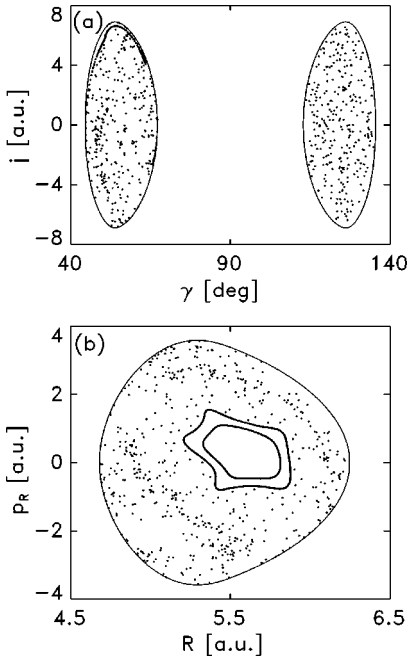

FIG. 5. Poincaré surfaces of section (γ,j) [a] and (R,p_R) [b] for several trajectories at $E=70\,cm^{-1}$. In each frame, three trajectories are shown.

The energy of the PSOS in Fig. 5, $E=70\,cm^{-1}$, is very close to the energy of the lowest vibrational vdW state ($E_0\approx 73\,cm^{-1}$). Thus, the classical phase space corresponding to the ground state is to a large extent chaotic, the exception being a region around the stable bending periodic orbit. Additional calculations show that the phase space is fully regular only near the vdW minimum and already 20 cm^{-1} above it the irregular trajectories dominate.

Let us now consider the vdW phase space at higher energies. One problem stands in the way of applying the PSOS technique above the saddle point on the path leading to the main ozone well: The vdW dynamics is no longer bounded and classical trajectories can escape from the vdW region to form ''normal'' ozone. Finite—and often short—lifetime obscures the representation of the phase space with the surfaces of section. The distinction between regular and chaotic dynamics becomes less clear, because many trajectories leave only a few traces on the PSOS. In order to demonstrate that the vdW dynamics is irregular also above the saddle, we consider the PSOS as a map and follow the subsequent iterations on this map. The idea behind this is to construct an analog of Arnold's ''cat map'' often used to illustrate the concept of the ''translation and stretching'' mixing in Hamiltonian systems.[33] The results of this procedure for the PSOS at $E=90\,cm^{-1}$ are summarized in Fig. 6. In the upper frame, Fig. 6(a), all the points are collected at which trajectories cross the PSOS *for the last time* before they escape into the main ozone well. At moderately high energies above the saddle, these points form a compact area. It provides a visualization of the ''exit gate'' or ''dynamical bottleneck'' previously studied in the photodissociation dynamics and reactive scattering.[34,35] One can relate this ''bottleneck'' to the

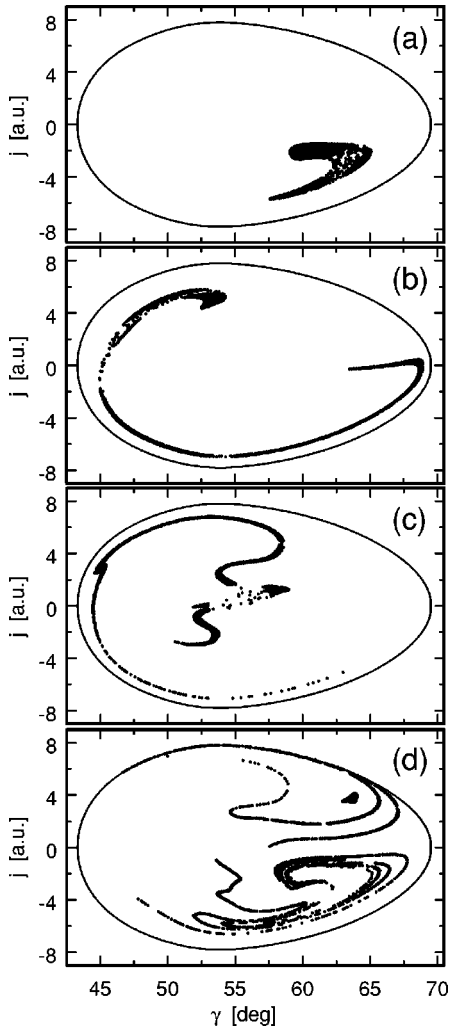

FIG. 6. Back-iterations of the Poincaré map (R,p_R) at $E=90\,\mathrm{cm}^{-1}$. See text for details.

bundle of trajectories surrounding the path connecting the vdW minimum with the saddle.[35]

We now follow the evolution of the area in Fig. 6(a) back in time and study its transformations as the map is *back-iterated*. Shown in Fig. 6(b) is the same ensemble of trajectories at the next to the last intersection with the PSOS. The compact area of the ''exit gate'' is strongly deformed after a single back iteration. If the trajectories were regular, the shape of the ''exit gate'' would remain largely unchanged: In a regular region, the time evolution of the trajectories amounts to a mere rotation around the periodic orbit. In contrast, the ''exit gate'' in Fig. 6(b) is transformed into a long and thin filament. This implies that the ensemble of trajectories passes through chaotic regions and is subject to contractions and expansions. The effect of these transformations becomes even more clear in the back iterations shown in Figs. 6(c) and 6(d) (third and fourth back iterations, respectively). The initial compact area quickly transforms into a set of long threads which fill almost randomly a large portion of the surface of section. The same picture holds qualitatively true for all energies above the saddle, although with increasing energy the ''exit gate'' gradually becomes less compact than in Fig. 6(a).

Comparison of different frames in Fig. 6 suggests that the successive back iterated images of the ''exit gate'' densely wrap around each other. This means that two neighboring points recombine into O_3 in different times: The lifetime depends strongly on the initial conditions. Extreme sensitivity of the dynamics to the initial conditions is known to be one of the hallmarks of chaos. This conclusion is further illustrated in Fig. 7. In Fig. 7(a), a composite PSOS (γ,j), produced by 10 000 trajectories, is shown. All trajectories were launched from the same point in the configuration space ($R^*=5.29a_0$, $\gamma^*=54.2°$) with randomly chosen magnitude and direction of the angular momentum j, so that the initial conditions are uniformly distributed along the dashed line in Fig. 7(a). In the middle frame, Fig. 7(b), the recombination lifetime of these trajectories is shown as function of the initial momentum j. Except for the interval $j\in[-5,0]$ a.u., the lifetime strongly fluctuates over two orders of magnitude even for neighboring initial conditions. These fluctuations are fingerprints of the filaments, discussed above, which densely intertwine in the phase space. The near fractal structure of the lifetime distribution is revealed in Fig. 7(c), which shows a portion of the same distribution for a smaller interval of j. The distribution is self-repeating: Neither the appearance of the curve nor the range of fluctuations change as observation scale is diminished.

The results in Fig. 7(b) show that at least one region remains less chaotic than the rest of the phase space: The lifetime dependence on j is smooth for $j\in[-5,0]$ a.u. Comparison between the frames (a) and (b) in Fig. 7 shows that trajectories with these initial momenta do not cross the PSOS (γ,j) calculated with the additional requirement $p_R>0$. Their lifetime is about 1.5 ps, i.e., it is of the order of one vibrational period in the vdW well. These trajectories are thus purely ballistic: They start from the vicinity of the vdW minimum with the initial momentum $p_R<0$ pointing in the direction of the saddle and quickly recombine into the main

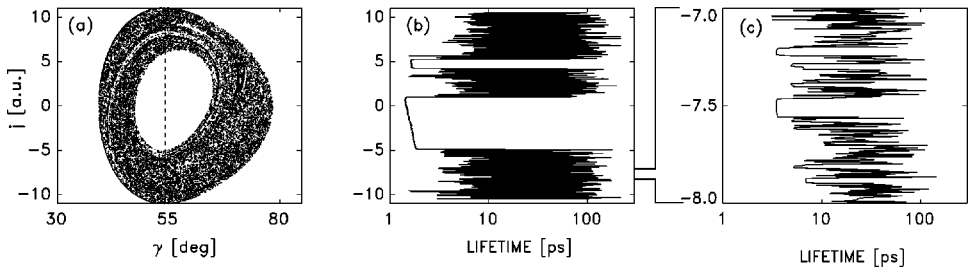

FIG. 7. (a) Composite surface of section (γ,j) obtained by integration of 10 000 trajectories at $E=80\,\mathrm{cm}^{-1}$. Initial conditions of all trajectories are uniformly distributed along the vertical dashed line. (b) The lifetimes of these trajectories versus the initial momentum j. (c) Zoom-in of the lifetime dependence on j for the interval $j\in[-8.0,-7.0]$ a.u. Logarithmic scale is used for the lifetimes in (b) and (c).

ozone. We argue in the next section that such short-living trajectories have no quantum mechanical counterpart.

V. QUANTUM/CLASSICAL CORRESPONDENCE IN VDW OZONE

In this section, we compare the properties of the classical and quantum dynamics of the vdW ozone. The present semiclassical study provides yet another indication that the quantum/classical correspondence is a subtle notion which depends on the level of details one is willing to compare and on the objects selected for such comparison.

The wave functions of vdW ozone have a very simple nodal structure which allows relatively straightforward assignment in terms of stretching and bending quantum numbers. The eigenstates preserve this simplicity throughout the spectrum, from the bottom of the vdW well to the dissociation threshold. In accord with this observation, semiclassical quantization with the periodic orbits with the shortest periods is successful. At this level of description, the agreement between quantum and classical mechanics is satisfactory.

At the same time, the quantizing POs are very often unstable. This is stressed in Fig. 4, in which the black dots on the stability curves for different families of POs mark energies of the eigenstates quantized by this family. No less than 2/3 of the quantum states are quantized by unstable orbits. However, no influence of the stability on the accuracy of the quantization was found (see Table I). The analysis of the phase space in the previous section demonstrates that instability of the selected short-period POs reflects a general property of the classical vdW motion. Namely, the classical motion is not integrable, but chaotic. This finding contradicts both the assignability of the quantum wave functions and the assumptions of the semiclassical quantization rule. Note that a similar observation was made in the study of the quantum/classical correspondence in HOCl close to the dissociation threshold.[36]

This discrepancy might be considered as a purely academic issue, as long as the semiclassical quantization works. Remember, however, that the vdW dynamics is metastable—with respect to the main ozone well—at all energies above the ground vibrational state. One can surmise that the regular quantum mechanical states and the chaotic classical trajectories recombine into normal ozone in different fashions. In what follows, we compare the quantum and classical recombination lifetimes of the vdW states.

In quantum mechanics, the lifetime τ_{qm} is estimated from the width of a resonance state, Γ, using the relation

$$\tau_{\mathrm{qm}}=\hbar/\Gamma. \tag{6}$$

The widths of the vdW states with respect to recombination into ozone are calculated using absorbing boundary conditions[37,38] in the *inner* part of the global ozone potential. The primary purpose of our calculations is to illustrate the quantum/classical correspondence in the vdW region of the potential. Usually, absorbing potentials are used in the asymptotic part of the PES in order to imitate the outgoing boundary conditions for an irreversibly decaying molecule. vdW states are only metastable if one vdW region is considered, as in the present paper. In the full calculations on the global PES these states are truly bound.[14] The decay from the portion of the potential restricted to one dissociation channel can be approximately considered irreversible because the main ozone well, acting as a ''sink'' for the states localized in the asymptotic region, is almost 9000 cm^{-1} deep, much deeper than the vdW well ($\sim$200 cm^{-1}).

The effective Hamilton operator in these calculations has the form $\hat{H}_{\mathrm{eff}}=\hat{H}_{\mathrm{3D}}-iW$. The complex absorbing potential $-iW$ vanishes in the vdW region $R\in[4.3,16.0]a_0$ and increases smoothly from zero at $R=4.3a_0$ to a maximum value at $R=3.5a_0$. The full 3D Hamiltonian, Eq. (1), is used because the adiabatic 2D Hamiltonian [Eq. (4)] was not calculated for $R<4.2a_0$. However, since both 2D and 3D spectra practically coincide, the resulting widths can be considered as a reasonable estimation for both operators. Complex eigenstates, $E_0-i\Gamma/2$, of the effective Hamiltonian are found using filter diagonalization, in which the propagator is expanded in modified Chebyshev polynomials.[39] Parameters of the propagation are similar to those described in Sec. II. The influence of the absorbing potential on the *real* parts of the eigenenergies is negligible: The energy shift due to $-iW$ does not exceed 0.1 cm^{-1}. Imaginary parts of the complex eigenenergies are transformed into lifetimes by use of Eq. (6).

Classical metastable dynamics of the vdW ozone is investigated by running trajectories on the 2D PES $\epsilon_0(R,\gamma)$ [cf. Eq. (4)] at seven energies ranging from $E=90\,\mathrm{cm}^{-1}$ (i.e., 10 cm^{-1} above the saddle to the main well) to $E=190\,\mathrm{cm}^{-1}$ (i.e., 15 cm^{-1} below dissociation threshold). At each energy, 10 000 trajectories are propagated for the maximum time of 220 ps. The trajectory is stopped after it had crossed the saddle in the direction of the main ozone well (the critical distance is $R=4.2a_0$). The time τ_k of the crossing is the lifetime of the kth trajectory. The distribution of lifetimes in the ensemble is represented in the form of a normalized ''survival probability'' $P(t)$,[40]

$$P(t)=10^{-4}\sum_{k=1}^{10\,000}\Theta(\tau_k-t), \tag{7}$$

where $\Theta(x)$ is a Heaviside step function. The classical lifetime, $\tau_{\mathrm{cl}}(E)$, for a given energy E is defined as the time, at which $P(\tau_{\mathrm{cl}})=1/e$.

Three types of the initial ensembles of trajectories are considered at each energy. The first is the microcanonical ensemble: The initial conditions for trajectories uniformly fill the phase space classically available at energy E. The second is the ''stretching'' ensemble: The initial conditions are chosen in a close vicinity of the stretching PO families. These trajectories start from the PSOS (γ,j), and their initial conditions are selected from a tiny square of the size $\delta\gamma=\delta j=0.05$ a.u. centered on the stretching PO. The third is the ''bending'' ensemble, in which the initial conditions cluster around the POs from the bending families. The ''bending'' ensemble starts from the PSOS (R,p_R), and the deviations from the bending PO are limited by $\delta R=\delta p_R=0.05$ a.u.

The quantum mechanical and the classical lifetimes, obtained in these calculations, are depicted in Fig. 8. The quantum recombination lifetimes fluctuate over several orders of magnitude, especially at low energies. These state- or mode-

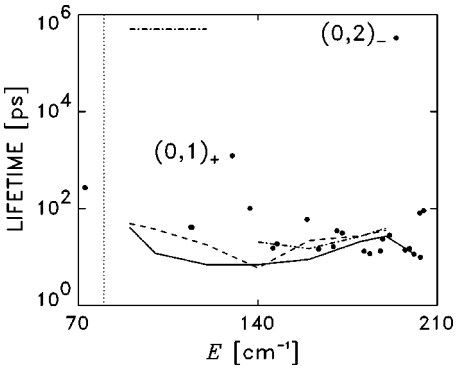

FIG. 8. Quantum mechanical (dots) and classical (lines) recombination lifetimes of vdW states of ozone. Classical lifetimes are shown for three ensembles of the initial conditions: microcanonical (solid line); ''stretching'' (dashed); and ''bending'' (dashed–dotted). See text for details. Vertical dotted line marks the position of the potential barrier between the vdW and the main ozone wells.

specific fluctuations were thoroughly analyzed in unimolecular dissociation reactions[41] and, therefore, are not surprising. The quantum recombination rate is sensitive to the exact shape of the wave function in the vdW wells and, in particular, to the probability density at the saddle (i.e., at the transition state). Since this density differs noticeably from progression to progression, and even from state to state within one progression, the lifetimes fluctuate. Only the first two (degenerate) states are located below the saddle and their lifetimes are due to tunneling through the potential barrier. The lifetimes of the states above the saddle can nevertheless be very long, reaching the range of microseconds. This is the effect of the adiabatic trapping previously discussed in Ref. 14: The zero-point energy of the bending mode at the transition state effectively increases the height of the dynamical barrier for the quantum particles passing into the main well. The largest are the lifetimes of the states belonging to the pure bending progression (Fig. 8); the lifetimes of the stretching states are shorter by four orders of magnitude. All quantum lifetimes exceed 10 ps, i.e., the states live for 4–5 vibrational periods before recombination.

It is clear from Fig. 8 that classical trajectories provide a reasonable estimation of the average recombination lifetime at high energies. This can be considered as another justification of the choice of the absorbing boundary conditions in the inner part of the potential for the quantum mechanical calculations. Consider the microcanonical ensemble first. At low energies ($E \leqslant 150\,\mathrm{cm}^{-1}$) the microcanonical lifetime is smaller than the quantum mechanical one by factors of 5–10. Apparently, the adiabatic barrier which hinders recombination of the quantum mechanical states does not affect the classical trajectories. As the energy increases, the microcanonical ensemble describes the average quantum lifetime better, with the best agreement achieved at dissociation threshold. Note, however, that the nonchaotic ballistic trajectories, described at the end of Sec. IV (see also Fig. 7), have no counterpart among the quantum states: The ''ballistic'' lifetimes, $\sim$1.5 ps, are one order of magnitude smaller than the smallest quantum lifetime.

Figure 8 shows that, being quite accurate ''on average,'' classical trajectories do not reflect the state specificity of the quantum mechanical lifetimes. Consider the lifetimes of the ''stretching'' and the ''bending'' ensembles. The classical lifetime depends on the size of the island of stability around the PO in question. At low energies, the two ensembles give different sets of lifetimes (Fig. 8, $E \leqslant 140\,\mathrm{cm}^{-1}$). The island of stability around the $[\gamma]$ PO is larger than the size of the square, from which the initial conditions for the ensemble are selected. As a result, the lifetime for these trajectories is infinite. In Fig. 8, it is artificially set to 8×10^6 ps. In contrast, POs of the $[R]$ family are unstable at these energies, and their lifetimes are finite. Above 140 cm^{-1}, the island of stability around the POs from the $[\gamma]$ family disappears (cf. Fig. 4), and their lifetime becomes finite, too. At these energies, there is virtually no difference between the two ensembles: Their lifetimes are almost equal to that of the microcanonical ensemble. This is another indication that the classical vdW dynamics is chaotic and the recombination lifetimes do not depend much on the initial conditions. Because of the chaotic behavior, the classical trajectories are insensitive to the quantum fluctuations: neither in the stretching nor in the bending progressions.

VI. CONCLUSIONS

This paper presents the analysis of the recently discovered vdW states of ozone from classical, semiclassical, and quantum mechanical viewpoints. All 22 quantum vdW states lie in the energy range in which classical chaos is fully developed and spreads over almost all available phase space. Nevertheless, the quantum system is not expected to display the properties inherent to the chaotic systems, such as the GOE statistics of the level spacings or irregular nodal patterns. Indeed, level statistics is meaningless for a spectrum consisting of only 22 lines. The longest series of states contains only five quanta of excitation (the pure stretching progression) which by necessity keeps the nodal patterns simple.

It is challenging to study the quantum/classical corresponding for such a system. The main finding of this work is that the quantum mechanical spectrum is built on three families of periodic orbits. The results clearly show that among all varieties of POs existing in the system, only the orbits with the shortest periods are important for the quantum mechanics. They act as backbones of the wave functions even in the presence of the bifurcations and can be used to quantize the eigenstates with reasonable accuracy. These POs are unstable at most energies, with the associated stability times being of the order of or shorter than the periods of the POs. Several previous studies showed that ''stability during one period'' might be sufficient for the orbit to become important in the semiclassical description (see Ref. 42, in which a chaotic 2D quartic oscillator is quantized, or Ref. 36 devoted to the analysis of the dynamics of HOCl).

The discrepancy between the fully chaotic classical dynamics and the regular quantum mechanical wave functions suggests that classical calculations should be used with care for retrieving intrinsically quantum properties of the vdW states, such as, for example, the recombination lifetimes.

ACKNOWLEDGMENTS

Financial support by the Deutsche Forschungsgemeinschaft and the Fonds der Chemischen Industrie is gratefully acknowledged. M.J. and S.Yu.G. are indebted to A. Matzkin for many fruitful discussions on the quantum/classical correspondence. S.Yu.G. would like to thank M. Ivanov for stimulating discussions on the classical lifetimes of the vdW ozone. He is grateful to the Université Joseph Fourier for a visiting position and the members of the Laboratoire de Spectrométrie Physique for the friendly support during the stay in Grenoble.

APPENDIX: PERIODIC ORBIT QUANTIZATION OF THE vdW STATES

In this Appendix, we outline the grounds on which the semiclassical quantization rules used in Sec. III for unstable POs are based. Our arguments are far from being exhaustive, but they provide an insight into the details of the quantization procedure and also indicate the direction of future work.

It is convenient to start with the local Hamiltonian near a certain periodic orbit. Throughout the Appendix we use units $\hbar = m = 1$. Let the coordinate along the orbit be S, with the conjugate momentum P_S, and let ξ and p_ξ describe the coordinate and momentum for the transverse direction. Then, the classical Hamiltonian near the orbit assumes the form,[43]

$$H_{\rm loc} = \tfrac{1}{2}P_S^2 + U(S) + \tfrac{1}{2}(p_\xi^2 + \omega_\xi^2 \xi^2), \tag{A1}$$

where $U(S)$ is the potential energy along the PO, and ω_ξ is the frequency in the transverse direction. Note that this frequency can, in general, be a function of S.

The energy of a state with quantum numbers $(n_S, n_\xi = 0)$ can be found from the quantization conditions of the local Hamiltonian (A1), if the quantum mechanical wave function is strongly localized around the orbit $(S, \xi = 0)$. One might further identify the frequency ω_ξ with the stability frequency of the orbit,[43,44]

$$\omega_\xi \approx \omega_{\rm st}. \tag{A2}$$

If the orbit is stable, so that its stability frequency, $\omega_{\rm st}$, is real, one immediately obtains from Eqs. (A1) and (A2) the semiclassical energy levels (see, for example, Ref. 45),

$$E_{\rm sc}(n_S, n_\xi = 0) = E_S(J = n_S + \tfrac{1}{2}) + \tfrac{1}{2}\omega_{\rm st}(E_S). \tag{A3}$$

Here J is the action along the orbit, and the function $J_S(E)$ and its inverse, $E_S(J)$ are assumed to exist. The stability frequency in Eq. (A3) is estimated at the energy of the orbit E_S.

The quantization rule (A3) breaks down for unstable orbits.[46] Indeed, the stability frequency for them is imaginary, and the transverse oscillator in Eq. (A1) supports no bound states. As a result, the semiclassical energy becomes complex and loses its meaning: The local approximation, Eq. (A1), is incompatible with the condition (A2). Possible solutions might consist of refining the local approximation and considering higher-order terms in Eq. (A1) or in abandoning the local form altogether.

The shape of the quantum mechanical wave functions in Fig. 2 suggests an alternative approach to the quantization along the unstable POs. All wave functions in the pure progressions are strongly localized around the orbits, irrespective of whether the POs are stable or not. Moreover, these wave functions in the direction transverse to the PO are simple bell-shaped Gaussian-type profiles. These observations suggest that one can keep the Hamiltonian near the PO in the form (A1), but redefine the transverse frequency in it. Consider the progression $(n_S, n_\xi = 0)$ and the orbit S. The following definition of the transverse frequency appears appropriate:

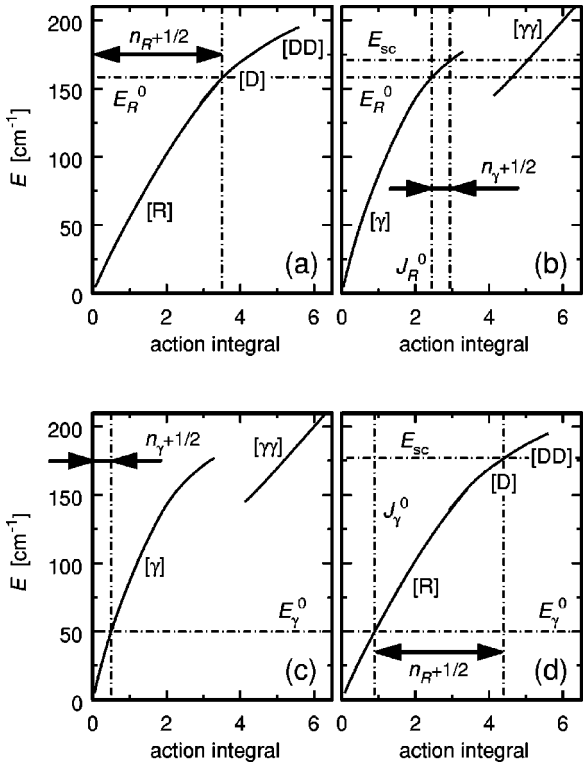

FIG. 9. Energy-action curves for the stretching [(a) and (d)] and bending [(b) and (c)] families of POs. The frames (a) and (b) are used to estimate the semiclassical energy with Eq. (A7); the frames (c) and (d) are used in Eq. (A8). See text for details.

$$\omega_\xi \approx \omega_{\perp \rm PO}. \tag{A4}$$

Here $\omega_{\perp \rm PO}$ denotes the frequency of *another* orbit, selected by the condition that it quantizes the states in the other pure progression $(n_S = 0, n_\xi)$. In some sense, this orbit, when properly chosen, plays the role of the ''transverse'' coordinate in the expansion (A1). At the same time, Eq. (A1) can no longer be considered as a local expansion: This is a model global Hamiltonian, which mimics the main features of the quantum wave functions (i.e., the Gaussian localization around the orbit S) but ignores the local details of the dynamics of this PO (i.e., its instability). The quantization rule then becomes

$$E_{\rm sc}(n_S, n_\xi = 0) = E_S(J = n_S + \tfrac{1}{2}) + \tfrac{1}{2}\omega_{\perp \rm PO}(E_S). \tag{A5}$$

This equation can be directly applied to the vdW spectrum of ozone. The bifurcation diagram, Fig. 3, unambiguously identifies the POs of the stretching families as being transverse to those of the bending families. Using the dependencies $J_S(E)$ (see Fig. 9), we calculate the semiclassical energies for the pure progressions $(n_R, n_\gamma = 0)$ and $(n_R = 0, n_\gamma)$. The results

are summarized in Table I. The accuracy of Eq. (A5) is rather high: For many states, the error is of the order of the tunneling splitting between the levels (note that tunneling effects are completely neglected in the above quantization rule). Inadequately described are only the highest stretching excitations $(5,0)_{+/-}$ and the circular state $(4,0)_C$. Incidentally, we note that for the circular state, a PO from the $[C]$ family was taken as the ''longitudinal'' orbit S and a PO from the $[\gamma\gamma]$ family served as a ''transverse'' orbit.

The above formula allows an extension to the combination states. Simultaneously, this extension somewhat improves the overall quality of the quantization, especially for the low lying levels. To be specific, let us assume for a moment that the orbit S belongs to the family $[R]$. We denote its energy $E_S(J=n_S+1/2)$ as E_R^0. The transverse PO belongs to the family $[\gamma]$. Equation (A5) can now be rewritten through E_R^0 and the functions $J_\gamma(E)$ and its inverse, $E_\gamma(J)$,

$$E_{sc}=E_R^0+\left[\frac{\partial E}{\partial J_\gamma}\right]_{J_\gamma^0}\Delta J_\gamma, \tag{A6}$$

where the frequency of the $[\gamma]$ PO, $\partial E/\partial J_\gamma$, is evaluated at $J_\gamma^0=J_\gamma(E_R^0)$, according to Eq. (A5). If the action increment, $\Delta J_\gamma=J_\gamma-J_\gamma^0$, equals 1/2, one recovers the quantization condition (A5). One can view Eq. (A6) as the first two terms in the Taylor expansion of energy near the action J_γ^0. Going beyond the linear terms and summing up, one obtains

$$E_{sc}=E_\gamma(J_\gamma^0+\Delta J_\gamma). \tag{A7}$$

The increment ΔJ_γ equals 1/2, if $n_\gamma=0$. For $n_\gamma>0$, one has $\Delta J_\gamma=n_\gamma+1/2$. Equation (A7) can be illustrated graphically [see Figs. 9(a) and 9(b)]. Suppose a state (n_R,n_γ) is to be quantized. Using the function $E_R(J)$ in Fig. 9(a), one finds $E_R^0=E_R(n_R+1/2)$. Switching next to the dependence $E_\gamma(J)$ in Fig. 9(b), one determines $J_\gamma^0(E_R^0)$. Finally, an increment $n_\gamma+1/2$ is added to J_γ^0 and the semiclassical energy is read from the vertical axis in Fig. 9(b).

We are not done yet. Equation (A7) lacks symmetry. This is especially clear for combination states: For them, it is difficult to decide which orbit should be considered as ''longitudinal'' and which one as ''transverse.'' One can repeat the arguments which lead to Eq. (A7), but interchange the roles of $[R]$ and $[\gamma]$ POs, thus arriving to another semiclassical expression

$$E_{sc}=E_R(J_R^0+\Delta J_R), \tag{A8}$$

where J_R^0 is evaluated at the energy $E_\gamma^0=E_\gamma(n_\gamma+1/2)$ and $\Delta J_R=n_R+1/2$. Graphical illustration of Eq. (A8) is given in Figs. 9(c) and 9(d). The arithmetic average of the two semiclassical formulas is symmetric with respect to interchange of the two families of POs. Thus, we obtain the final quantization rule

$$E_{sc}=\tfrac{1}{2}[E_\gamma(J_\gamma^0+n_\gamma+\tfrac{1}{2})+E_R(J_R^0+n_R+\tfrac{1}{2})]. \tag{A9}$$

In the case of vdW states of ozone, the difference between the two predictions (A7) and (A8) is less than 10 cm^{-1}, and the average Eq. (A9) provides an accurate estimation of the quantum mechanical eigenenergies. The actual quantization uses different families of orbits at different energies. For example, when $[R]$ family ceases to exist, the action along the $[D]$ orbits is used as $J_R(E)$. Similarly, the $[\gamma\gamma]$ orbits are substituted for the $[\gamma]$ when the latter disappears (cf. Fig. 9). The circular state is quantized with the $[C]$ family. The results are summarized in Table I and discussed in Sec. III. For many states, Eq. (A9) is numerically superior to its nonsymmetric linearized counterpart, Eq. (A5). The accuracy is, however, still poor for the levels $(5,0)_{+/-}$. In general, the performance of the quantization is impaired (a) if the anharmonicity in the progression [i.e., the curvature of the $E(J)$ curve] is large, and/or (b) if a bifurcation creates a gap in the $J(E)$ dependence. The first circumstance is probably responsible for the discrepancies observed at higher excitations in R. The gap in the action between the $[\gamma]$ and $[\gamma\gamma]$ families leads to underestimation of the energies for $(0,2)_+$ and $(1,2)_+$ (see Table I). In the future, we plan to investigate more closely the effect of bifurcations and switching between different families of POs on the quantization condition (A9).

[1] *Molecular Quantum States at Dissociation*, edited by R. Prosmiti, J. Tennyson, and D. C. Clary [Collaborative Computational Project on Heavy Particle Dynamics (CCP6), Daresbury Laboratory, UK, 1998].
[2] H. Ishikawa, R. W. Field, S. C. Farantos, M. Joyeux, J. Koput, C. Beck, and R. Schinke, Annu. Rev. Phys. Chem. **50**, 443 (1999).
[3] M. Joyeux, S. C. Farantos, and R. Schinke, J. Phys. Chem. A **106**, 5407 (2002).
[4] T. Helgaker, P. Jorgensen, and J. Olsen, *Molecular Electronic-Structure Theory* (Wiley, Chichester, 2000).
[5] M. E. Kellman, in *Molecular Dynamics and Spectroscopy by Stimulated Emission Pumping*, edited by H.-L. Dai and R. W. Field (World Scientific, Singapore, 1995).
[6] M. S. Child, *Semiclassical Mechanics with Molecular Applications* (Clarendon, Oxford, 1991).
[7] M. S. Child and L. Halonen, Adv. Chem. Phys. **57**, 1 (1984).
[8] A. Delon and R. Jost, J. Chem. Phys. **95**, 5686 (1991).
[9] A. Delon, P. Dupre, and R. Jost, J. Chem. Phys. **99**, 9482 (1991).
[10] A. Delon, R. Georges, and R. Jost, J. Chem. Phys. **103**, 7740 (1995).
[11] J. Weiss, J. Hauschildt, S. Yu. Grebenshchikov, R. Düren, R. Schinke, J. Koput, S. Stamatiadis, and S. C. Farantos, J. Chem. Phys. **112**, 77 (2000).
[12] D. A. Sadovski, N. G. Fulton, J. R. Henderson, J. Tennyson, and B. I. Zhilinski, J. Chem. Phys. **99**, 906 (1993).
[13] T. Azzam, R. Schinke, S. C. Farantos, M. Joyeux, and K. A. Peterson, J. Chem. Phys. **118**, 9643 (2003).
[14] S. Yu. Grebenshchikov, R. Schinke, P. Fleurat-Lessard, and M. Joyeux, J. Chem. Phys. **119**, 6512 (2003).
[15] E. J. Heller, Phys. Rev. Lett. **53**, 1515 (1984).
[16] M. Founargiotakis, S. C. Farantos, G. Contopoulos, and C. Polymilis, J. Chem. Phys. **91**, 1389 (1989).
[17] J. Bredenbeck, C. Beck, R. Schinke, J. Koput, S. Stamatiadis, S. C. Farantos, and M. Joyeux, J. Chem. Phys. **112**, 8855 (2000).
[18] R. Jost, M. Joyeux, S. Skokov, and J. Bowman, J. Chem. Phys. **111**, 6807 (1999).
[19] K. Mauersberger, Geophys. Res. Lett. **8**, 935 (1981).
[20] Y. Q. Gao and R. A. Marcus, Science **293**, 259 (2001).
[21] K. Mauersberger, D. Krankowsky, C. Janssen, and R. Schinke, Adv. At. Mol. Phys. (in press).
[22] P. Fleurat-Lessard, S. Yu. Grebenshchikov, R. Siebert, R. Schinke, and N. Halberstadt, J. Chem. Phys. **118**, 610 (2003).
[23] R. Schinke, P. Fleurat-Lessard, and S. Yu. Grebenshchikov, Phys. Chem. Chem. Phys. **5**, 1966 (2003).
[24] P. Fleurat-Lesard, S. Yu. Grebenshchikov, R. Schinke, C. Janssen, and D. Krankowsky, J. Chem. Phys. **119**, 4700 (2003).
[25] A. Rohrbacher, N. Halberstadt, and K. C. Janda, Annu. Rev. Phys. Chem. **51**, 405 (2000).
[26] P. Rosmus, P. Palmieri, and R. Schinke, J. Chem. Phys. **117**, 4871 (2002).
[27] R. Siebert, P. Fleurat-Lessard, R. Schinke, M. Bittererova, and S. C. Farantos, J. Chem. Phys. **116**, 9749 (2002).
[28] M. R. Wall and D. Neuhauser, J. Chem. Phys. **102**, 8011 (1995).
[29] V. A. Mandelshtam and H. S. Taylor, J. Chem. Phys. **103**, 2903 (1995).

[30] J. Echave and D. C. Clary, Chem. Phys. Lett. **190**, 225 (1992).
[31] J. C. Light and T. Carrington, Adv. Chem. Phys. **114**, 263 (2000).
[32] S. C. Farantos, Comput. Phys. Commun. **1008**, 240 (1998).
[33] M. Tabor, *Chaos and Integrability in Nonlinear Dynamics* (Wiley, New York, 1989).
[34] M. J. Davis, Int. Rev. Phys. Chem. **14**, 15 (1995).
[35] H. Wadi and L. Wiesenfeld, Phys. Rev. E **55**, 271 (1997).
[36] M. Joyeux, D. Sugny, M. Lombardi, R. Jost, R. Schinke, S. Skokov, and J. Bowman, J. Chem. Phys. **113**, 9610 (2000).
[37] G. Jolicard and E. J. Austin, Chem. Phys. **103**, 295 (1986).
[38] T. Seideman and W. H. Miller, J. Chem. Phys. **96**, 4412 (1992).
[39] T. P. Grozdanov, V. A. Mandelshtam, and H. S. Taylor, J. Chem. Phys. **103**, 7990 (1995).
[40] S. K. Gray, S. A. Rice, and M. J. Davis, J. Phys. Chem. **90**, 3470 (1986).
[41] S. Yu. Grebenshchikov, R. Schinke, and W. L. Hase, in *Comprehensive Chemical Kinetics*, edited by N. J. B. Green (Elsevier, Amsterdam, 2003), Vol. 39.
[42] B. Eckhardt, G. Hose, and E. Pollak, Phys. Rev. A **39**, 3776 (1989).
[43] G. Vattay, Phys. Rev. Lett. **76**, 1059 (1996).
[44] The stability parameters $\lambda_{1,2}$, discussed in Sec. IV, can be expressed through the stability frequency ω_{st}: $\lambda_{1,2}=\exp(\pm i\omega_{st}T)$, where T is the period of the PO. For a stable PO, the stability parameters are complex, while the stability frequency is real. For an unstable PO, the stability parameters are real, and ω_{st} is purely imaginary.
[45] W. H. Miller, J. Chem. Phys. **63**, 996 (1975).
[46] A. Voros, J. Phys. A **21**, 685 (1988).